

M. Keilhacker
and the JET Team

Fusion Physics Progress in the JET Joint Undertaking

Fusion Physics Progress in the JET Joint Undertaking

M. Keilhacker
and the JET Team^{*}

JET Joint Undertaking, Abingdon, Oxfordshire, OX14 3EA,

^{*} See Annex

"This document is intended for publication in the open literature. It is made available on the understanding that it may not be further circulated and extracts may not be published prior to publication of the original, without the consent of the Publications Officer, JET Joint Undertaking, Abingdon, Oxon, OX14 3EA, UK".

"Enquiries about Copyright and reproduction should be addressed to the Publications Officer, JET Joint Undertaking, Abingdon, Oxon, OX14 3EA".

ABSTRACT

The paper discusses recent progress in fusion physics on the Joint European Torus (JET) in the fields of plasma confinement, MHD stability, particle and power exhaust, and fusion performance and α -particle effects. In this context results are presented from the three JET operating regimes: ELM-free H-mode, ELMy H-mode and optimised shear mode. These results together with those from other tokamaks form a sound basis for extrapolation to a Next Step device based on ELMy H-mode operation and point the way for the development of more advanced tokamak scenarios.

1. INTRODUCTION

Progress in fusion physics has to be measured against the physics requirements of a Next Step device and a future fusion reactor. While most requirements of a reactor plasma have already been met individually it is still necessary to bring all these together in a coherent concept for the plasma core and the plasma edge/divertor. The physics issues of a tokamak plasma can be divided into four main areas: plasma confinement, MHD stability, particle and power exhaust, and fusion performance and α -particle effects. These areas are intimately linked with each other and one cannot be optimised without impacting on another. In the following the physics progress that has been made on the Joint European Torus (JET) over the last few years in each of these areas is discussed.

JET has three main operating regimes: The ELM-free H-mode [1] which produces the highest performance but is transient in nature, the ELMy H-mode [2] which allows long, steady pulses and is the standard operating mode foreseen for ITER and finally the optimised (reversed) shear mode [3] which has the potential for high β and steady-state operation and is the mode envisaged for the second phase of ITER operation. Progress in the understanding of transport and MHD stability in each of these operating regimes is discussed, while divertor studies have been carried out mainly under ELMy H-mode conditions.

Finally, it is worth noting the unique position of JET for contributing to the physics understanding required for ITER or any other Next Step device by virtue of its ITER geometry (non-circular plasma cross-section, bottom single null divertor), its large size which brings it closest to ITER in all scaling experiments, and its D-T and Remote Handling capability which make it the only experiment world-wide able to study the physics processes with the isotope mixture of a reactor and to carry out isotope scaling studies.

2. CONFINEMENT PROJECTIONS AND LIMITATIONS

The ELMy H-mode is the standard operating mode foreseen for ITER FDR and is the only steady-state regime which has been experimentally validated. "Wind Tunnel" scaling experiments, in which the important dimensionless parameters for confinement were matched to those of ITER, predict ignition for ITER provided the required densities can be reached and source and profile shapes can be preserved. This may not be a valid assumption since transport barriers can

exist and their properties must be studied in order to determine their affect on profiles and, hence, overall confinement. Two such transport barriers are considered, in the plasma edge and interior, where confinement is improved towards neoclassical levels and MHD stability limits can be approached.

2.1 Global Projections

ITER demonstration pulses preserve all the relevant dimensionless parameters (such as the normalised plasma pressure β_N , collisionality ν^* and the edge safety factor q_{95}) close to the values of an ignited ITER, except for the normalised plasma size (the dimensionless Larmor radius, $\rho^* = \rho_i/a$). On JET, the level of additional heating power prevents such demonstration pulses being produced at the highest level of performance, but at lower toroidal field and plasma current (e.g. 2 T/2 MA), the β_N (2.4) and collisionality of an ignited ITER [4] have been closely matched and q_{95} was also close to the ITER value ($q_{95}=3.2$). Such a JET discharge in D-T forms the basis of a series of ‘‘Wind Tunnel’’ experiments (Fig. 1) [5] which are found to scale close to gyro-Bohm and extrapolate to ignition in ITER. In fact, a gyro-Bohm extrapolation from this ITER demonstration pulse gives ignition at 1.8 GW (or $Q=5.8$ for a Bohm extrapolation) for ITER operating at 21 MA. The required density would, however, be 50% above the Greenwald density limit which scales as I/a^2 .

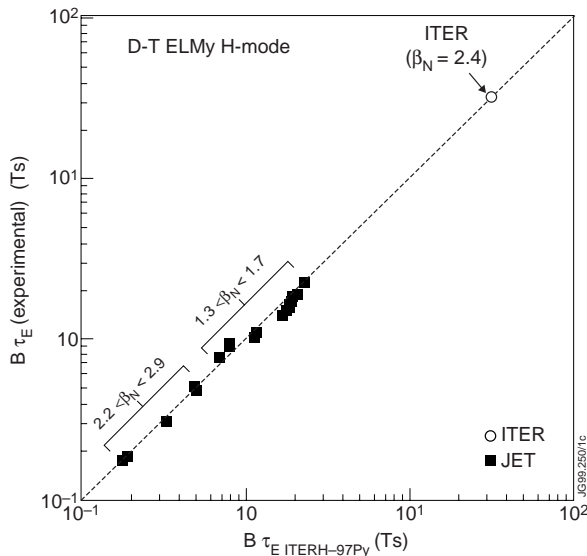


Fig. 1 Measured thermal energy confinement times of ITER similarity ELMy H-mode discharges in D-T plotted against the scaling law used in ITER projections. The operating point of an ignited ITER is also shown.

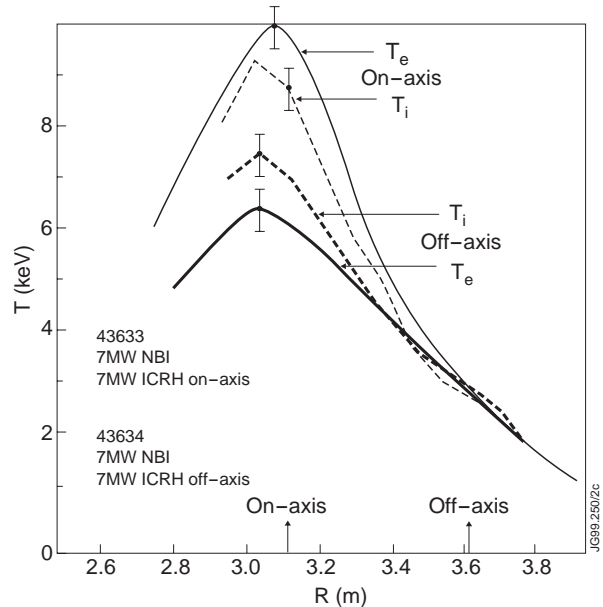


Fig. 2 Electron and ion temperature profiles for on- and off-axis ICRF heating, showing that the core temperature profiles respond to the changes in heating.

2.2 Source and Profile Dependency

In JET, the plasma temperatures respond to changes in the heating profile. Figure 2 shows clearly the response of the electron and ion temperatures to the application of on- and off-axis Ion Cyclotron Resonance Frequency (ICRF) heating during the sawtooth-free phases of Neutral

Beam (NB) heated ELMy H-mode discharges at low density. Thus, a simple local transport model (e.g. $\chi \propto |\nabla T|^\alpha$) is adequate to describe energy transport in the plasma core and the stored plasma energy and, hence, global confinement is different in the two cases.

2.3 Effect of Transport Barriers on Energy Confinement

The total thermal energy of an ELMy H-mode plasma can be separated into two contributions [6]: a pedestal energy (Fig. 3(a)) which is determined from the edge temperature and density (assuming equal electron and ion temperatures at the plasma edge); and a core energy (Fig. 3(b)) which is determined by subtracting the pedestal energy from the total energy. These contributions are found to scale differently with respect to mass and other significant parameters. The scaling of the pedestal energy has been obtained from a free fit, constrained to specific physics models. A particularly good fit is to a model which assumes that the gradient of the plasma pressure in the edge is limited by ideal ballooning mode instabilities over a distance characterised by an ion Larmor radius [6]; this leads to a positive mass dependence ($A^{0.5}$), as shown in Fig. 3(a). The best fit is with thermal ions. The corresponding core energy confinement time (Fig. 3(b)) is found to be consistent with the $A^{-0.2}$ mass dependence which would be expected from a pure gyro-Bohm scaling, generic of theoretical transport models based on turbulence with a scale length of the ion Larmor radius.

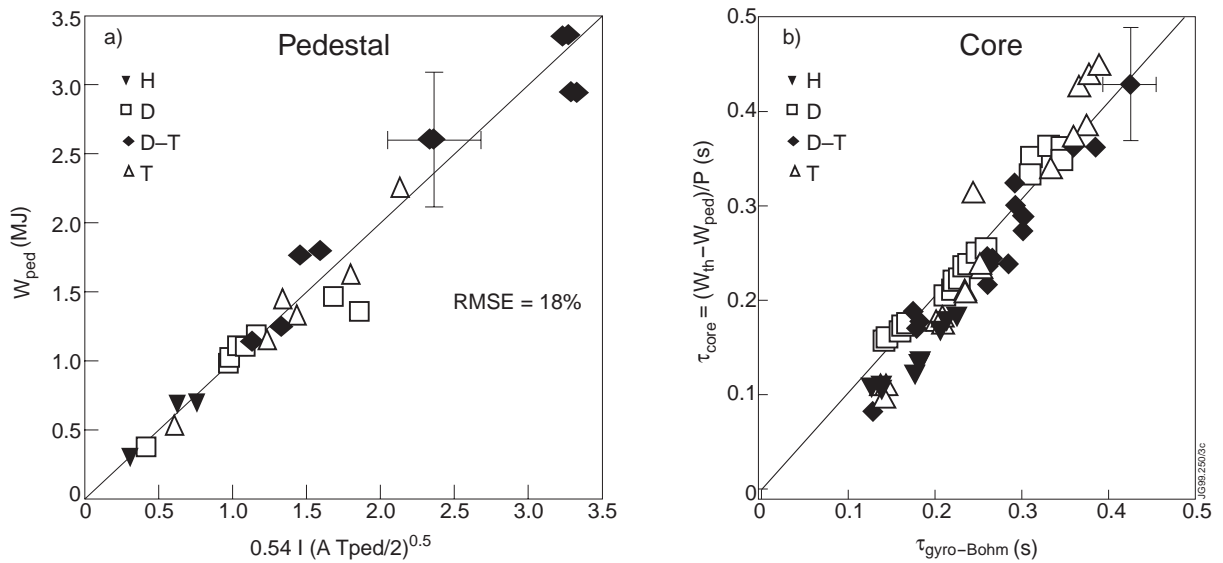


Fig. 3 a) Pedestal energy plotted against that expected from an edge pressure gradient limited by ballooning modes over an ion poloidal Larmor radius and b) the thermal confinement time of the core plasma plotted against the best fit for the mass dependence in a pure gyro-Bohm scaling for ELMy H-mode discharges in hydrogen, deuterium, deuterium-tritium and tritium.

An expression for the total energy confinement time may then be obtained by adding the two contributions. In dimensionless form this expression can be written as [6]:

$$\omega_c \tau_E \propto \langle \rho \rangle^{*-3} (1 + c \langle \rho \rangle^{*2} / \beta_N^2) \quad (1)$$

The core contribution, being consistent with gyro-Bohm scaling, would be favourable for

extrapolations to a reactor; the pedestal scaling shows degradation with decreasing temperature, e.g. increasing density and/or radiated power, but requires the scale length for the edge transport barrier to be determined before it can be used with confidence for extrapolations to a reactor. For the ITER FDR design parameters [4] equation (1) predicts a global energy confinement time of 4.8s compared to 5.8s using the ITERH-EPS97(Y) scaling expression [7]. This should still allow ignition although with reduced margins.

2.3.1 H-mode Threshold Power

JET experiments in hydrogen, deuterium, tritium and D-T mixtures have allowed the effect of isotope mass on the H-mode threshold power to be determined. The most notable result is that, in comparison with pure deuterium, the H-mode threshold power was lower in D-T and lower still in pure tritium, scaling roughly as the inverse of the atomic mass (A^{-1}) of the plasma mixture. This can be seen in Fig. 4(a) which shows the loss power from the plasma plotted against ITER scaling for the H-mode threshold power [8] modified to include an inverse mass dependence.

These results reduce significantly the power requirements for ITER to access the H-mode: in a pure tritium plasma (for example, during the start-up phase when it is important to achieve the H-mode as early as possible) the power is reduced by 33%, while in a 50:50 mixture of deuterium and tritium the power is reduced by 20%.

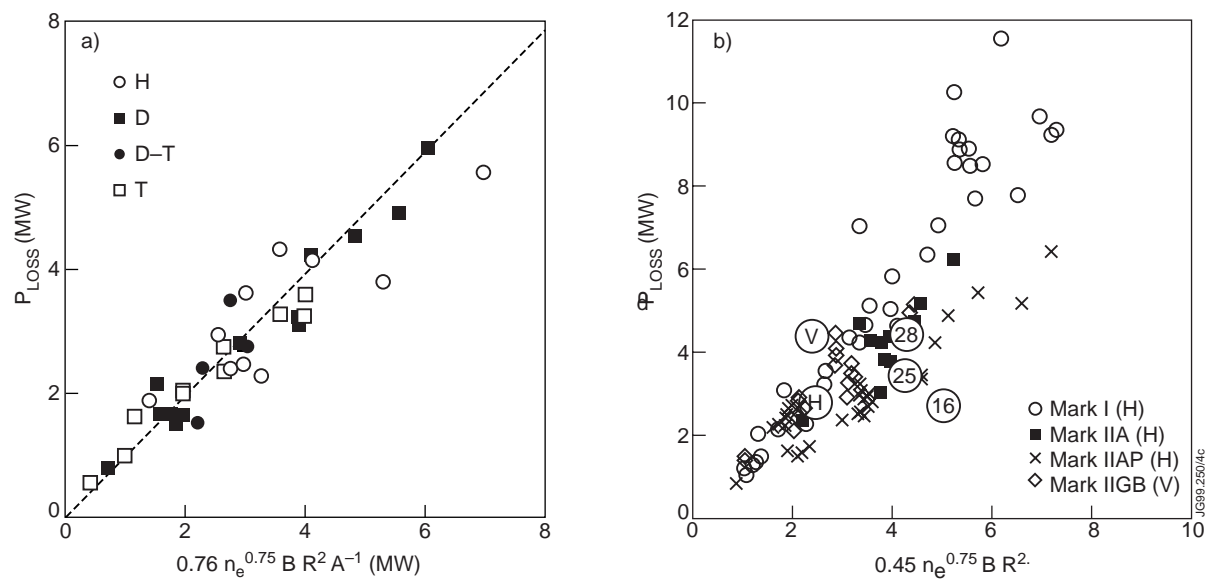


Fig. 4 Dependence of H-mode threshold power on a) isotope mass and b) divertor geometry.

JET experiments have also shown that the H-mode threshold power is dependent on the geometry of the divertor [9]. In particular, as shown in Fig. 4(b), the threshold decreases with increasing divertor closure (Mark I \rightarrow Mark IIAP) and is higher with vertical targets (V \rightarrow H with Mark IIAP). Furthermore, results with the Mark IIGB divertor show that configurations with the X-point close to or on the septum have a lower than normal threshold; understanding these differences should elucidate the physics basis for the L-H transition.

2.3.2 Internal Transport Barriers

The first observation of Internal Transport Barriers (ITBs) was made in JET PEP-mode plasmas in 1988 [10, 11]. Shear reversal was obtained in the PEP regime using injected pellets of solid deuterium. The standard method of producing ITBs today is in the optimised Shear (OS) regime [3] in which a current ramp of $\approx 0.4\text{MA/s}$ and early heating to slow current penetration provide flat or hollow current density profiles. The main heating phase (NB plus ICRF heating) is then timed such that $q_0 \leq 2.0$; if a threshold power is exceeded, an ITB forms. As shown in Fig. 5, the minimum power at which an ITB forms in JET OS discharges increases with toroidal magnetic field. To obtain a strong ITB and high performance requires, however, 40 to 60% more power and since the total heating power in JET is limited to about 24MW operation at the highest magnetic field (4.0T), where performance is best, is restricted. Most studies were therefore done at 3.4T and below; for recent results see [12-14].

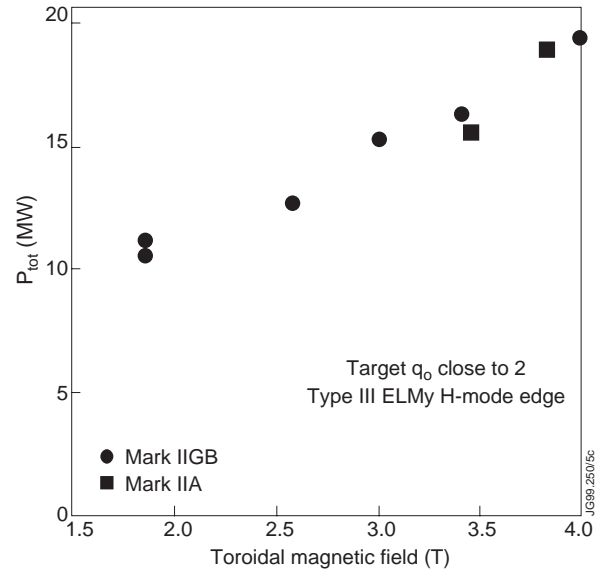


Fig. 5 Threshold power for internal transport barriers in discharges with the Mark IIA and Mark IIGB divertors.

The formation of an ITB is known to result in reduced core plasma energy transport and it is believed that this may occur through a combination of ExB velocity shear and magnetic shear stabilisation of plasma turbulence [15]. Recent studies on JET OS discharges using a system of X-mode reflectometers capable of measuring density fluctuations across the whole plasma diameter have revealed that the turbulence suppression occurs in two stages (Fig. 6) [16]. First, low frequency, long wave length turbulence is suppressed throughout the plasma core by toroidal velocity shear generated by the intense auxiliary heating. Then, when the ITB forms, high frequency, short wavelength turbulence is suppressed locally within the steep pressure gradient region of the ITB by ExB poloidal shear (positive feedback between enhanced ∇p and ExB shear). Spatially, the turbulence can be separated into three regions (Fig. 6c): Outside the ITB (edge), within the ITB gradient, and inside the ITB (core). The initial low frequency suppression occurs right across the plasma core out to the ITB foot and is associated with a strong reduction of the ion heat conductivity which drops towards neoclassical values at the barrier and stays low throughout the core (Fig. 7). The high frequency suppression, on the other hand, is restricted to the narrow ITB gradient region and results in a localised drop of the electron heat conductivity in this region (Fig. 7).

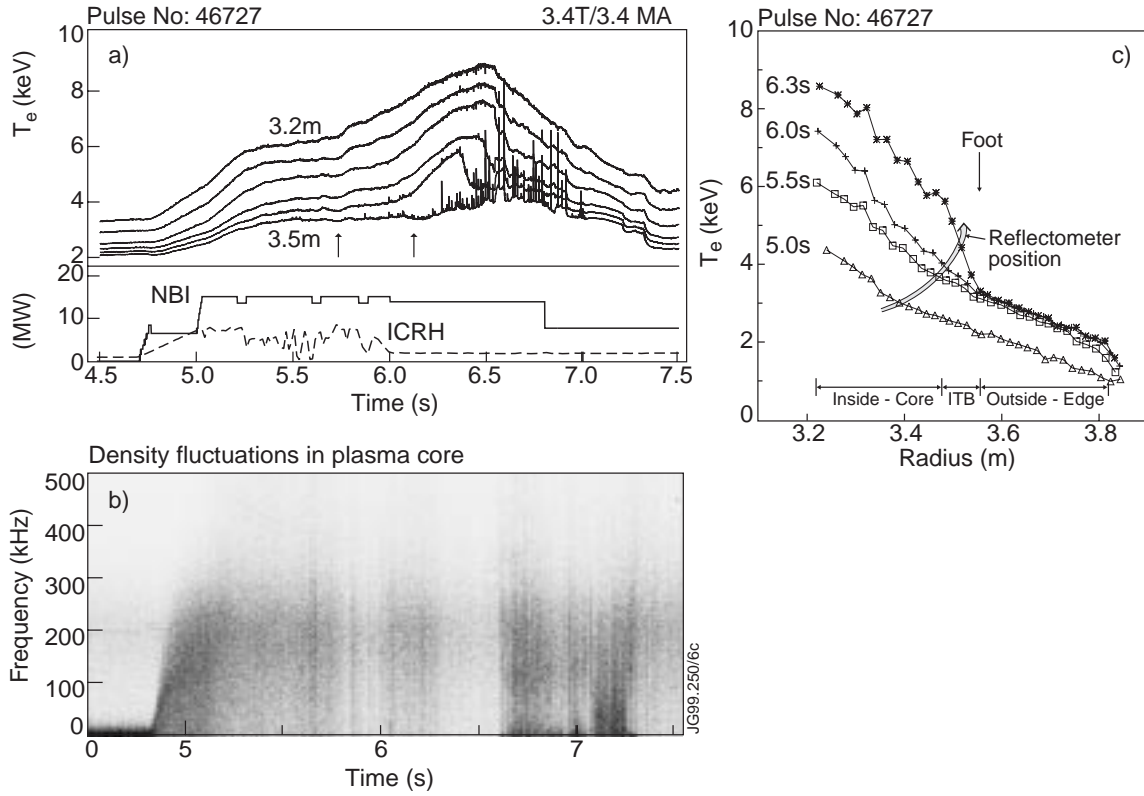


Fig. 6 a) Time traces of electron temperature at various radial locations, b) spectrum of core density fluctuations and c) electron temperature profiles showing turbulence suppression and ITB formation during an optimised shear discharge.

3. MHD INSTABILITIES AND THEIR AVOIDANCE

MHD instabilities can limit performance in all JET operating regimes. In ELMy H-mode plasmas neoclassical tearing modes can lead to a modest reduction in confinement. In ELM-free H-mode and optimised shear discharges MHD instabilities, correlated with the location of the peak pressure gradient, can pose a fundamental limit to high performance: in ELM-free H-mode plasmas the large pressure gradients at the plasma edge lead to edge instabilities, whereas in optimised shear discharges the large core pressure gradients, which coincide with a region of relatively low shear, make the plasma core prone to instabilities. These instabilities have to be avoided to allow steady-state high performance to be reached.

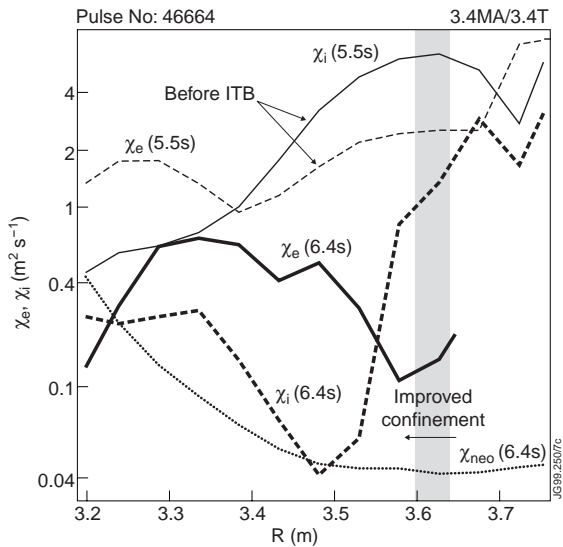


Fig. 7 Thermal diffusivities before and after ITB formation showing a strong reduction of χ_i across the plasma core inside the ITB and a local drop of χ_e within the ITB region.

3.1 Neoclassical Tearing Modes in ELMy H-mode Discharges

Neoclassical tearing modes (NTM) are a critical issue for Next Step devices since they can limit β in ELMy H-mode discharges (the standard scenario for ITER) to values well below the limit set by ideal MHD instabilities. They occur at high enough β_N when an MHD perturbation, such as a sawtooth, triggers a sufficiently large seed island.

At JET NTMs have been observed at medium to high β_N (between 2 and 3) in long pulse ELMy H-mode discharges (Fig.8a) [17] although such discharges can also exist without such modes up to $\beta_N \approx 2.6$. The modes are mostly triggered by a large sawtooth crash (at $\beta_N = 3.0$ in Fig. 8a) and persist throughout the heating phase. After the appearance of the mode sawteeth are suppressed in general and the electron temperature profile is flattened locally around the $q=1.5$ surface indicative of the formation of an island. NTMs depress the plasma performance although in JET their effect on the confinement time is relatively modest (a reduction of 5-20%).

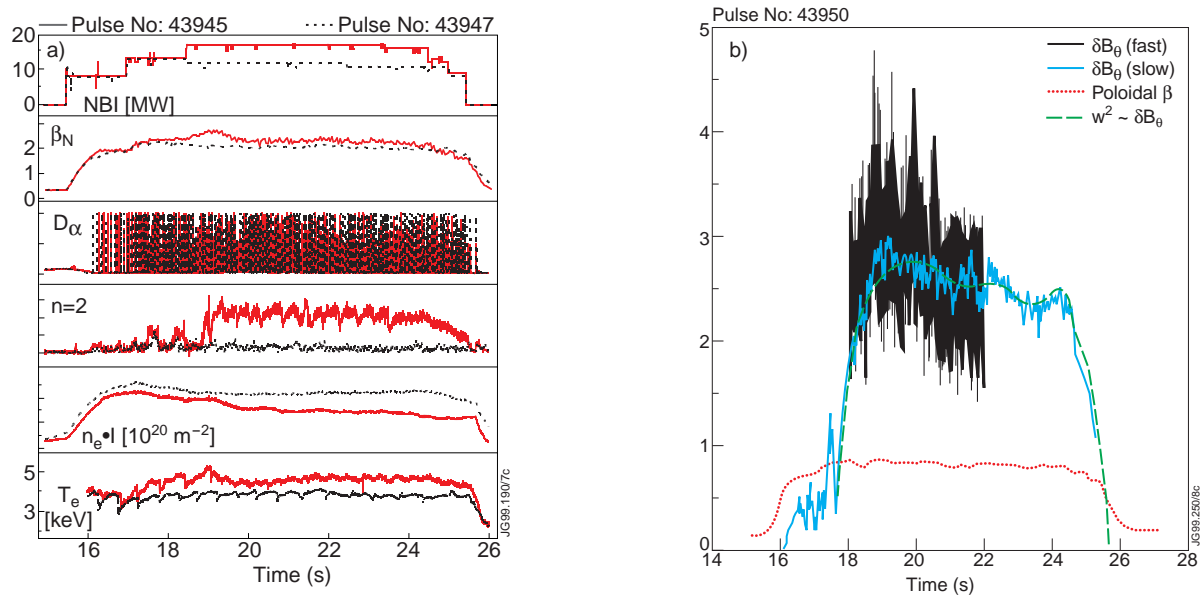


Fig. 8 a) Example of a long pulse ELMy H-mode discharge (1.7T/1.7MA) with an $n=2$ mode triggered by a sawtooth at $\beta_N = 2.65$ and comparison with a similar discharge with lower heating power in which the $n=2$ mode is stable at $\beta_N = 2.1$ and b) experimental and modelled evolution of island width.

In JET these modes have been observed with fast ECE diagnostics (sampling rate 250 kHz) and with SXR cameras (178 viewing lines), the latter allowing a detailed tomographic reconstruction of the perturbation of the SXR emission in the poloidal plane. This reconstruction shows that the toroidal mode number of the perturbation is predominantly $n=2$ with coupled $m=2$ and $m=3$ poloidal harmonics [17]. The amplitude of the mode is much larger on the low field side, where the $m=2$ and $m=3$ components add up, than on the high field side. Both diagnostics show the perturbation to be a relatively global mode.

Modelling the evolution of the magnetic perturbation (i.e. the island size) as a function of time using modified neo-classical theory yields good agreement with the measurements (Fig. 8b)

[17,18]. This shows that the plasma pressure is the driving force of the $n=2$ mode and identifies it as a neo-classical tearing mode as opposed to a tearing mode driven by the current density gradient.

A database containing discharges obtained with the Mark IIA [17] and Mark IIGB [18] divertors shows that the value of β_N at the onset of the NTM scales strongly with the normalised Larmor radius ρ^* ($\propto \rho^{*0.6}$) but has only a weak, negative dependence on v^* ($\propto v^{*-0.1}$) (different to the scaling $\beta_N \propto v^{*0.3}$ found on DIII-D [19]). A similar scaling with ρ^* (linear in ρ^*) was found in AUG [20].

3.2 External Kink Modes in ELM-free H-mode Discharges

In the ELM-free H-mode the large pressure and current density gradients in the plasma edge can drive Outer Modes (localised in the outer 20% of the plasma) and ELMs. A comparison of the reconstructed SXR data of the outer mode with predictions based on the mode structure of an ideal $n=1$ external kink mode shows excellent agreement (Fig. 9), identifying the Outer Mode as an external kink mode [21]. Although outer modes are confined to the plasma periphery they cause a global degradation of energy confinement.

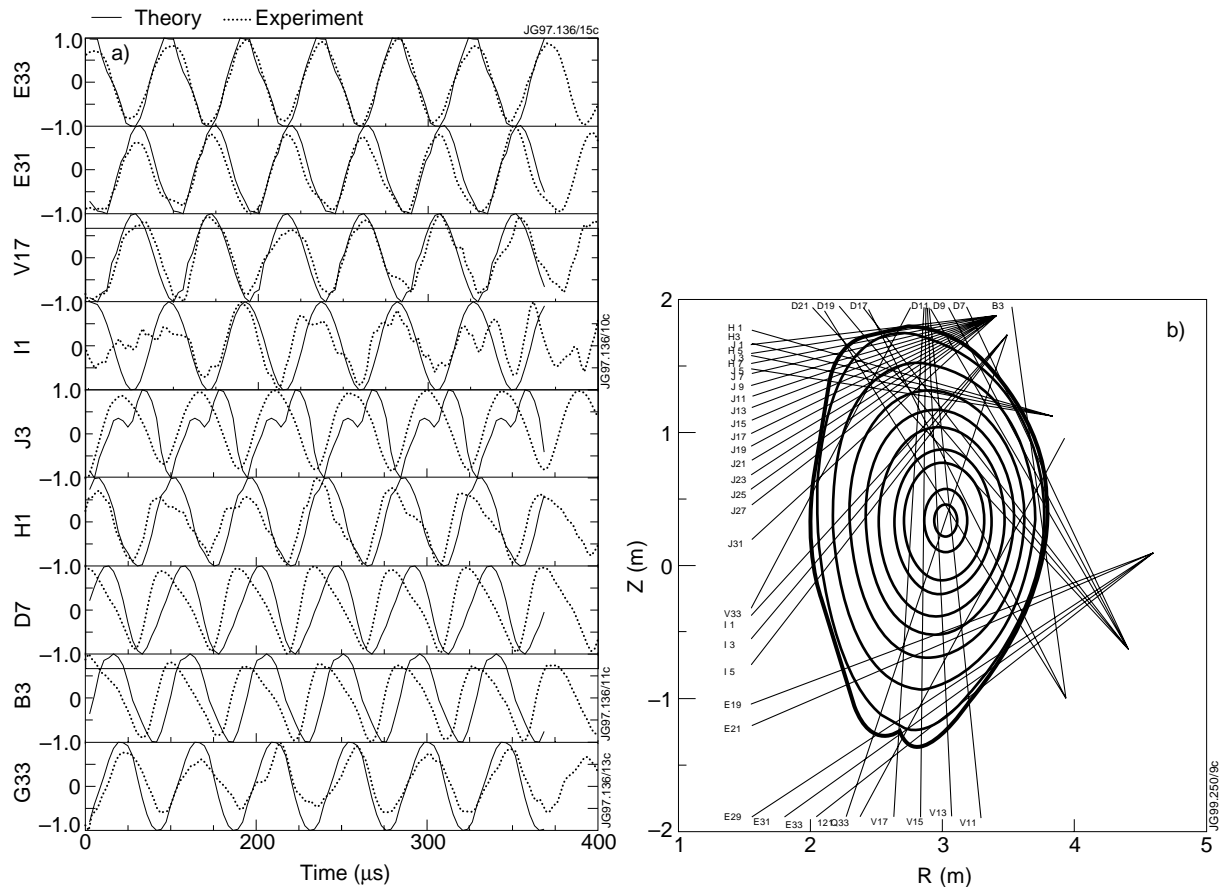


Fig. 9 a) Comparison of observed (in SXR emission) and predicted mode structures identifying the outer mode as an $n=1$ external kink mode and b) lines of sight of the SXR channels.

This detailed understanding of the Outer Mode and its identification as a current driven instability has suggested a way in which it might be controlled, namely by reducing the edge current density [22]. Fig. 10a shows that by ramping down the current just before the onset of the Outer Mode, the mode could be delayed, resulting in a considerable increase in neutron rate. A stability analysis (Fig. 10b) confirms the beneficial effect of the current ramp-down. As can be seen in the discharges in Fig. 10a the Outer Mode is usually followed by a Giant ELM which terminates the high performance phase. This occurs when the plasma edge comes close to the limit for ballooning instabilities (Fig. 10b).

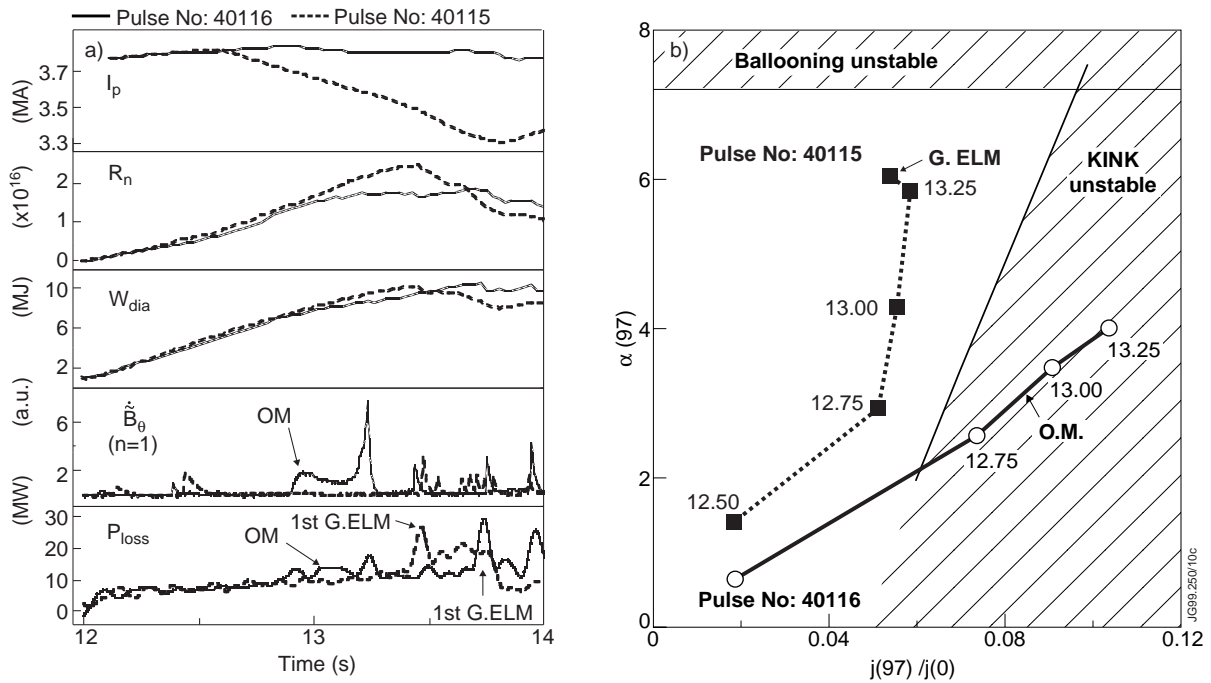


Fig.10 Delay of outer mode by current ramp-down and stability diagram confirming the stabilising effect of reducing the edge current.

3.3 Ideal Pressure Driven Kink Modes in Optimised Shear Discharges

The MHD instabilities that occur in the optimised shear (OS) regime are quite different from those observed in ELM-free H-modes. Sawteeth, one of the main performance limiting MHD instabilities in the H-mode regime, are absent because the minimum q is well above unity and the plasma edge is often in L-mode, thus avoiding the Outer Modes and Giant ELMs characteristic of the H-mode edge. The MHD instabilities of OS plasmas are related to the peaked pressure inside the ITB and the particular shape of the q profile with low central magnetic shear. The most common limitation to performance of JET OS discharges are disruptions which can occur at relatively low β_N ($1 < \beta_N < 2$). Other MHD phenomena that limit the performance are $n=2$ “snakes” which erode the ITB leading to energy losses that trigger an ELM-free period which in turn terminates the ITB.

Most disruptions are preceded by a clear precursor (Fig. 11a) which has the structure of a global ideal MHD mode with toroidal mode number $n=1$ [23]. In the example of Fig. 11a, the mode amplitude grows exponentially with a characteristic time of 0.2ms. As the mode grows the frequency slows down until it locks to the wall, at which point the plasma disrupts. The time from the start of the mode to the disruption is typically a few ms. The radial structure of the disruption precursor has been constructed using the data from the 48 channel heterodyne ECE radiometer. Fig. 11b shows the time evolution of the electron temperature profile inside the ITB at the time of the disruption precursor. In the last oscillation before the disruption the displacement of the flux surfaces due to the MHD instability causing the disruption grows to a large amplitude of ± 15 cm. A detailed inspection of the displacement of the flux surfaces shows that the disruption precursor is an ideal MHD mode [23].

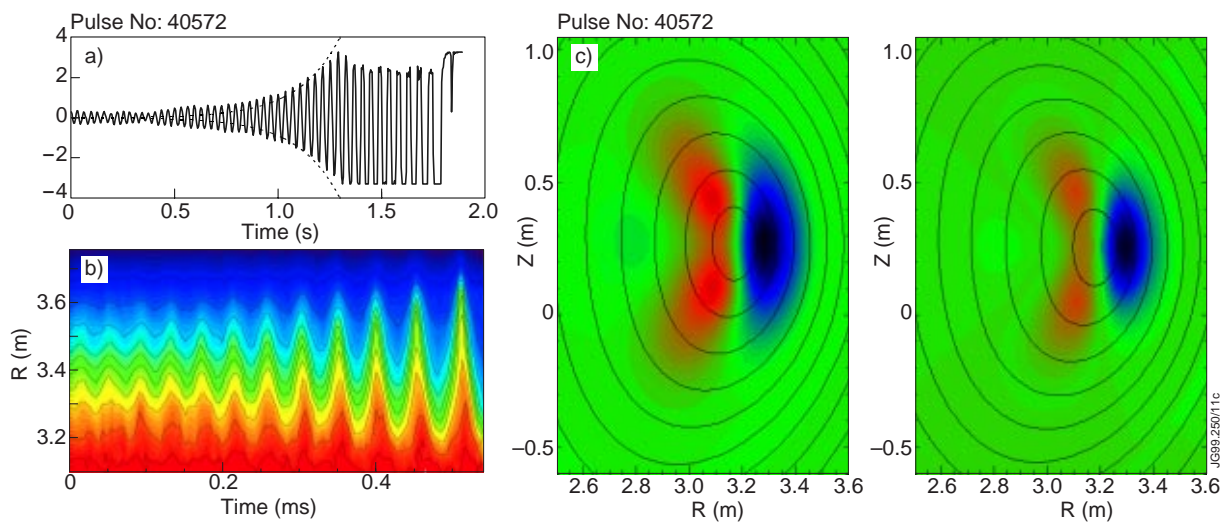


Fig.11 a) Disruption precursor as seen by a magnetic pick-up coil, b) electron temperature contours showing the precursor across region inside ITB and c) comparison of the $n=1$ perturbation of the SXR emission from tomographic reconstruction and from MHD calculations.

More information on the mode structure of the precursor has been obtained from tomographic reconstruction of the SXR emission. A detailed comparison of the observed mode structure with the results from ideal MHD stability calculations (Fig. 11c) shows that the disruption precursor is a global $n=1$ pressure driven kink mode which becomes unstable as the ideal MHD stability limit is exceeded [23]. The best performance in OS discharges has been obtained by operating the discharges very close to the MHD stability boundary using real time control of the heating power. Fig. 12a shows a pulse with the highest neutron rate (5.4×10^{16} n/s) in deuterium OS plasmas (with Mark IIA divertor). The ICRF power was reduced when the neutron rate reached 2×10^{16} n/s; after that the NB power was controlled to follow a prescribed neutron rate wave form. As can be seen from Fig. 12b the discharge was kept close to the MHD stability limit for more than 1 second (note that it seems necessary to include an ideal wall at the JET location in the stability analysis). Up to 6.8s the plasma was in L-mode but with a strong ITB; at 6.8s it went into H-mode which reduced the peaking factor of the pressure profile sufficiently to avoid a disruption.

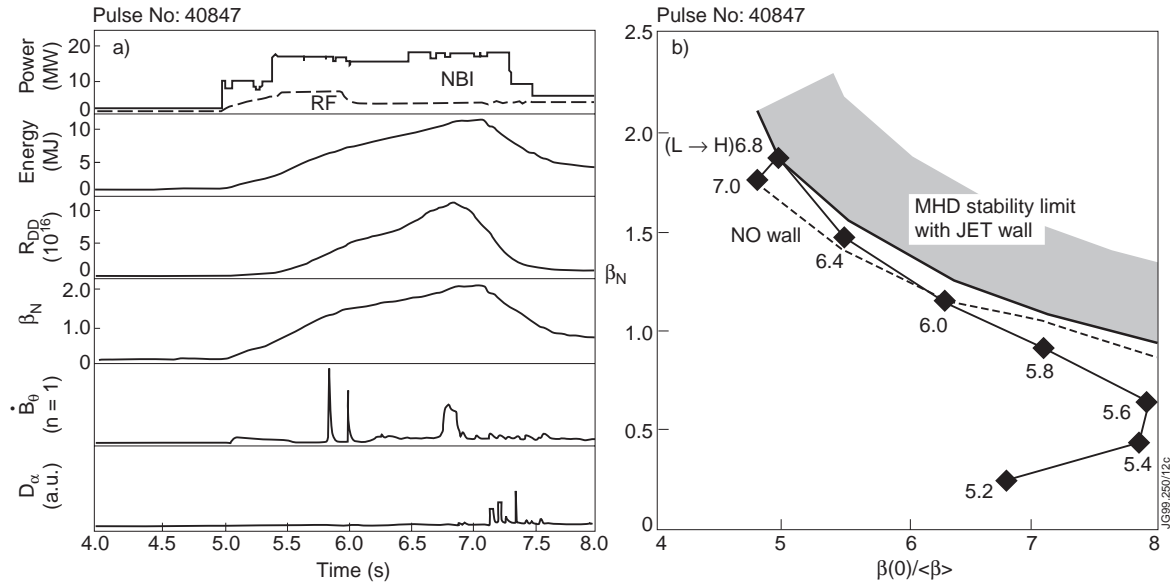


Fig. 12 a) Time traces of a high performance optimised shear discharge with real time control of heating power and b) stability diagram for this discharge showing avoidance of MHD stability limit.

Because of the fast growing nature of these disruptions, their avoidance is the only means of control. The main controls exercised so far are: slower heating to control the peaking of the pressure profile, and puffing of impurities - most notably Argon - to prevent large ELMs [24]. Fig. 13a shows a discharge (Pulse No. 47413) in which a combination of slower heating and Argon puffing has avoided a disruption (as in Pulse No. 46664) leading to a record pulse duration of 4 seconds. As seen in Figs. 13b and 13c, controlled discharges operate very close to their calculated (including effect of JET wall) stability limits and achieve higher β_N using less peaked pressure profiles than their disruptive counterparts.

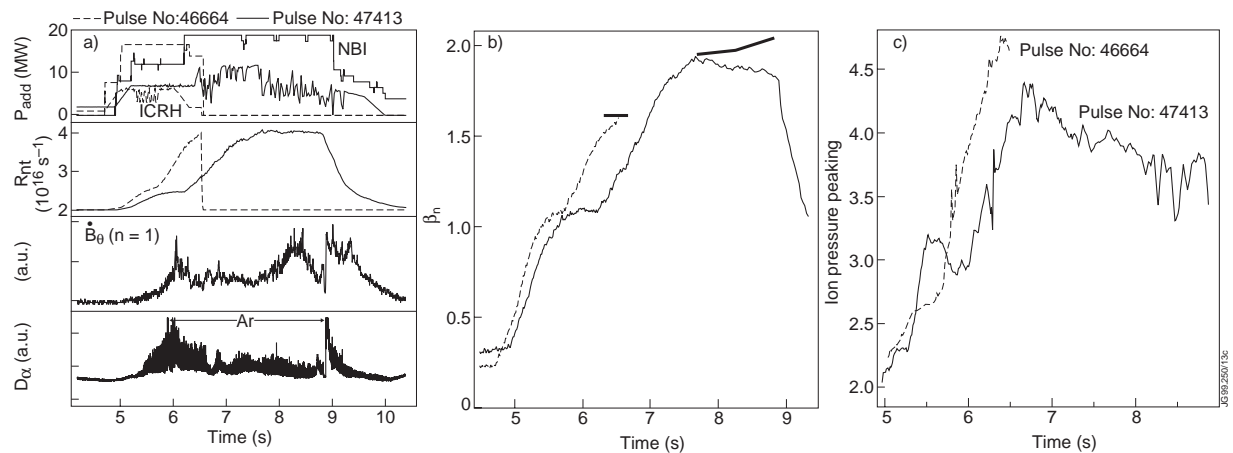


Fig. 13 Record duration high performance optimised shear discharge (Pulse No. 47413) and comparison with typical high performance disruptive discharge (Pulse No. 46664). a) Various time traces, b) discharge trajectories and calculated disruptive stability limits (thick lines) and c) evolution of pressure peaking.

4. PARTICLE AND POWER CONTROL

JET is the largest divertor experiment and for the last 8 years (1992-99) the development of a viable divertor concept for ITER/Next Step has been one of the main objectives of the JET Programme [25]. The two basic functions of a divertor are efficient particle control (for the hydrogen plasma, the helium ash and the impurities) and “safe” power exhaust (e.g. by reducing the power load to the target plates via radiation and CX neutrals in a “detached” plasma in the divertor chamber). This has to be achieved without deleterious effects on global confinement and bulk plasma performance.

4.1. Helium Exhaust

In recent experiments on JET the pumping speed for helium was varied by varying the amount of argon frosting used on the divertor cryopump [26]. Measurement of the global particle confinement time of helium, $\tau_p^*(\text{He})$, at various pumping speeds (Fig. 14a) allows extrapolation to the core particle confinement time (for infinite pumping speed) of helium, $\tau_p(\text{He})$, which for the ELMy H-mode discharges investigated is $\tau_p(\text{He}) = 1.3\text{s}$ (Fig. 14b). This leads to a ratio of helium particle confinement time to energy confinement time $\tau_p(\text{He})/\tau_E(\text{He}) \approx 4$, which is significantly lower than the value needed for reactor operation (<10 [27]). Similar results have also been obtained on ASDEX Upgrade [28] and DIII-D [29].

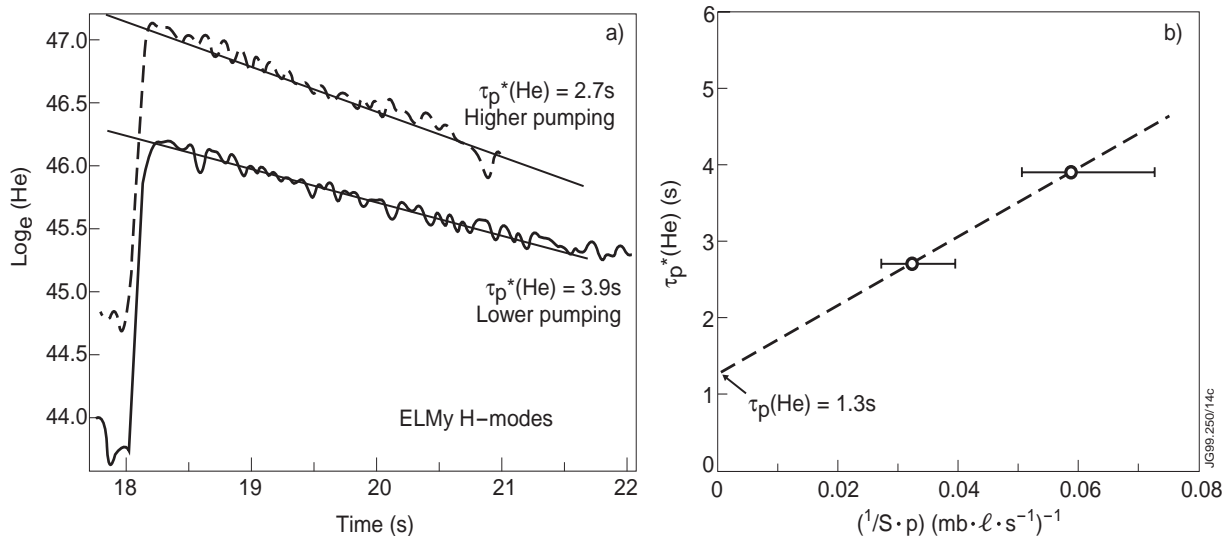


Fig. 14 a) Global particle confinement time of Helium, $\tau_p^*(\text{He})$, at two pumping speeds and b) extrapolation to the core particle confinement time, $\tau_p(\text{He})$ (at infinite pumping speed).

4.2 Detachment

Full or partial detachment is believed to be essential for safe power exhaust in ITER/Next Step. As seen in Fig. 15a, detachment is characterised by a large drop in plasma pressure (nT) in the divertor, which relates to a large drop in plasma energy. Extrapolation to ITER indicates that detachment should result in tolerable average divertor power densities. However, the very high transient power loads associated with ELMs could pose a problem for large devices like ITER (see section 4.3).

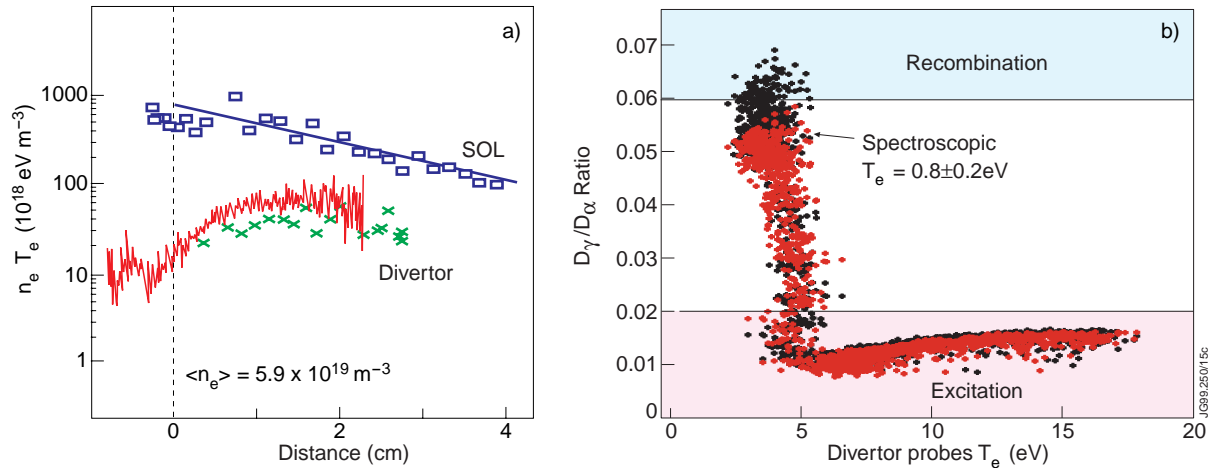


Fig. 15 a) Drop in divertor plasma pressure during detachment and b) spectroscopic signature of detachment showing correlation of detachment with strong recombination at temperatures below 1eV.

Over the last few years a good qualitative understanding of the physics processes leading to detachment has evolved. In particular, it has become clear that - in addition to radiation and CX neutrals - recombination plays an important role in the energy loss processes leading to detachment: first, line radiation cools the divertor plasma down from a few tens of eV, then at temperatures $T_e \leq 5 \text{ eV}$ momentum removal by neutrals becomes important, and finally for $T_e < 1 \text{ eV}$ strong recombination removes charged particles and energy (the neutral particles also spread the remaining power over a larger area). Fig. 15b shows that detachment is closely correlated with the spectroscopic signatures of recombination: the ratio of the Balmer lines D_γ/D_α rises sharply at the transition from the attached regime, characterised by electronic impact excitation which predominantly populates the lower states (D_α), to the detached regime, characterised by recombination with an increase in the relative population of the upper states (D_γ).

4.3 Impact of ELMs

Recent measurements with a fast IR camera on JET have confirmed previous observations that the time in which Type I ELMs deposit their power on the target plates is $\approx 100 \mu\text{s}$, which is shorter or comparable to the deposition time in smaller machines. Together with the observation of a nearly machine independent change in plasma energy $\delta W/W = 4\text{-}7\%$ per ELM, this would lead to peak energy and power loads for the ITER FDR divertor (plasma energy 950MJ, target area 10 m^2) of a few MJ/m^2 (important for erosion of target material) and up to a few 100GW [30]. This would be unacceptably high and shows the importance of developing more detailed ELM models to place the extrapolation to ITER on a sounder basis.

4.4 Sequence of Progressively More Closed JET Divertors

Over the last 8 years JET has pursued a three stage programme of progressively more closed divertors (Fig. 16) [25]: After installation of the divertor coils and divertor cryopumps in the JET vacuum vessel (1991/92), the JET divertor programme started with the relative open, but very

flexible Mark I divertor (1994/95). This was followed by the more closed Mark IIA divertor (1996/97) which also allowed a comparison of divertor operation on horizontal and vertical targets. Finally, in early 1998 the Mark IIA target structure was exchanged, solely by Remote Handling, with the most ITER-like Mark IIGB target structure which features a “Gas Box” type geometry and vertical targets as foreseen for ITER.

Divertor closure is expected to produce a number of beneficial effects: detachment should occur at lower density (or less impurity seeding), the divertor neutral pressure should increase (facilitating particle removal) and the neutral pressure in the main chamber should decrease (reducing the wall impurity source). All these effects have been observed as the JET divertors become progressively more closed. With increasing closure, detachment occurs at lower upstream densities (for a fixed power) and the pressure at the pump strongly increases (Fig. 17a). Figure 17b shows the effect of divertor closure on intrinsic impurities [31]. In L-mode plasmas impurity levels (Z_{eff}) decrease markedly from Mark IIA to the more closed Mark IIGB. This beneficial effect of closure on impurities is less pronounced in H-mode plasmas due to the ELMs producing additional large impurity sources outside the divertor.

4.5 Strong Intrinsic Scrape-off Layer Flows

For some time it has been a puzzle (and a disappointment) that Z_{eff} in JET could not be reduced further by “puff and pump” experiments designed to flush wall produced impurities into the divertor and to entrench impurities (e.g. seed impurities) originating in the divertor as was predicted in [32] and successfully demonstrated on DIII-D [33]. These JET results can now be understood following the observation of strong intrinsic flows (larger than the externally induced flows) in the scrape-off layer (SOL) of JET. A similar observation has been made on ASDEX Upgrade [34].

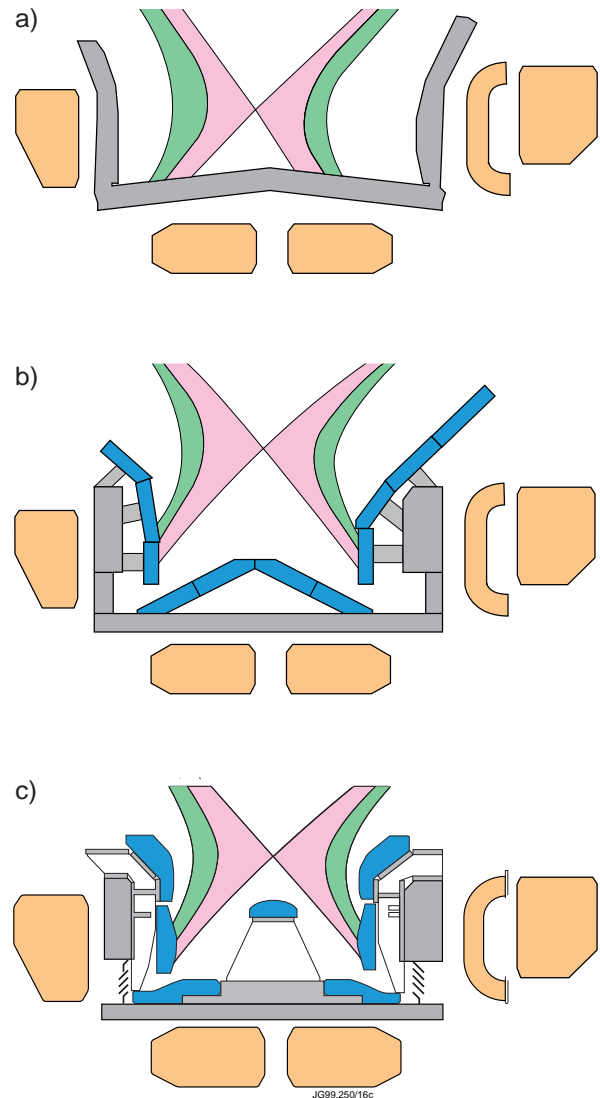


Fig. 16 Schematic poloidal cross-sections of the progressively more closed a) Mark I, b) Mark IIA and c) Mark IIGB divertors.

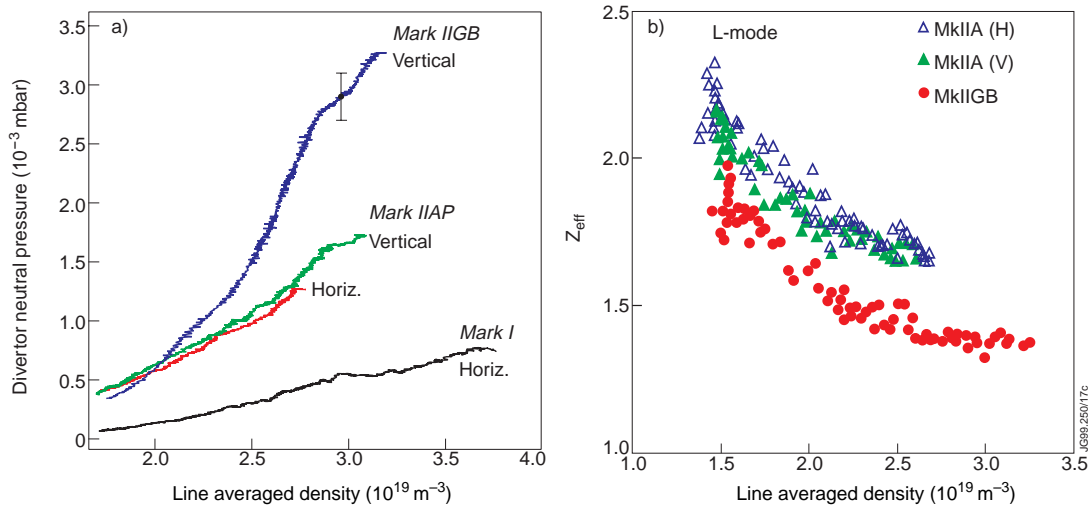


Fig. 17 Effect of divertor closure on a) divertor pressure and b) bulk plasma impurities (Z_{eff}).

Using a Mach Reciprocating Probe near the top of the torus (Fig. 18a) plasma flows in the SOL of JET L-mode discharges (Mark IIIGB) have been measured [35]. With “normal” toroidal field ($\mathbf{B} \times \nabla \mathbf{B}$ towards the lower single null divertor), the flows are from the outer to the inner divertor, with flow speeds up to $M=0.6$ (Fig. 18b). When the toroidal field and plasma current are reversed, the direction of the flow also reverses. These flows are probably caused by a toroidal rotation of the SOL plasma in the direction of the plasma current, superimposed on Pfirsch-Schlüter flows (this explanation is supported by preliminary EDGE2D transport code calculations).

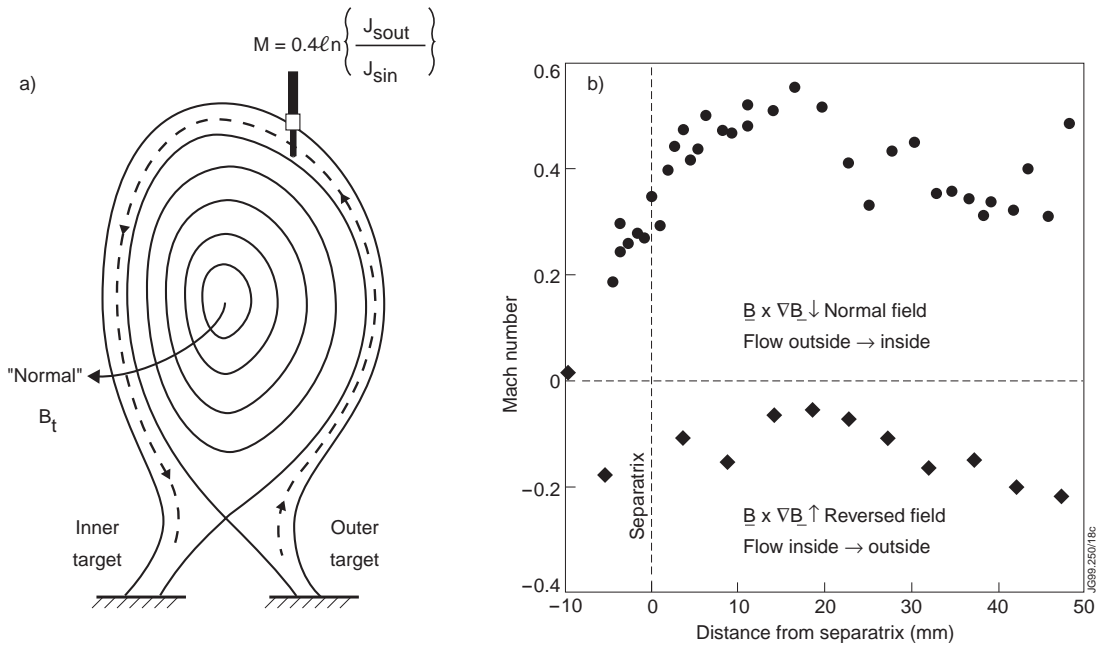


Fig. 18 a) Location of Mach Reciprocating Probe and b) strong flows observed in the JET scrape-off layer, from outside to inside with ‘normal’ magnetic field and in the opposite direction if magnetic field is reversed.

The SOL momentum results from neoclassical drifts: the $\nabla \mathbf{B}$ drift drives a radial current j_r

and the resultant $j_r B_\theta$ force accelerates the SOL in the toroidal direction. The observation that the flow does not completely reverse could be caused by (partial) flow reversal near the outer target due to ionisation and/or preferential perpendicular transport through the outer midplane (ballooning type transport) leading to higher pressure at the outside.

4.6 Scrape-off Layer Flows and Tritium Retention

The strong intrinsic SOL flows probably also explain the observation that at the end of the D-T campaign in 1997 (DTE1) about 6g tritium out of the 35g injected during DTE1 were retained in the vacuum vessel [36]. Inspection during the following shutdown showed that most of the tritium was retained in carbon flakes at the inner divertor louvres (Fig. 19). In general, the inspection showed strong asymmetries in the pattern of carbon deposition, with heavy deposition on the water-cooled louvres of the inner divertor and very little deposition at the outer divertor [30]. Such asymmetries cannot be predicted correctly by simple edge plasma modelling. However, a good match to the JET data can be obtained with the DIVIMP code if three extra physical processes are introduced [37]: enhancing the sputtering at the vessel wall by neutrals (in lieu of adding sputtering by ions which is presently not included in the code), introducing reflection for carbon atoms at the inner divertor target (supported by recent laboratory measurements [38], showing high C_2H_X release rates from hydrogen-rich amorphous films) and introducing a strong additional flow in the SOL from the outside to the inside as discussed in the previous section.

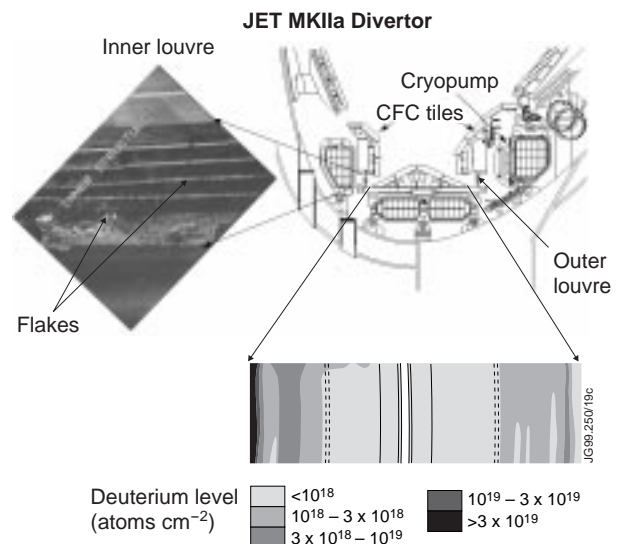


Fig. 19 Cross-section of the Mark IIA divertor, with insets showing the flaking deposition at the inner louvres and a plot of deuterium concentration on the floor-tiles.

5. FUSION POWER AND ALPHA PARTICLE EFFECTS

After the first ever production of significant fusion power (1.7MW) during the Preliminary Tritium Experiment (PTE) in 1991 [39], JET carried out a series of D-T experiments (DTE1) in 1997 which addressed a wide range of D-T physics and technology issues for ITER [36,40,41]. In the following the main physics results on ICRF heating, fusion power production and α -particle effects from the DTE1 campaign are summarised.

5.1 Test of ITER ICRF Heating Scenarios

The physics and performance of three ICRF schemes applicable to D-T operation in ITER and a reactor were tested successfully in ELMy H-mode discharges [42]. Figure 20 summarises the heating effect of these three schemes in a plot of central ion and electron temperatures versus

power per particle. The D and ^3He minority schemes generated strong bulk ion heating, whereas the second harmonic tritium ($2\omega_{\text{CT}}$) scheme heated mainly the electrons but is predicted to become an ion heating scheme under ITER conditions. Most of the ICRF heating results in D-T are in excellent agreement with PION code predictions, giving confidence in the use of these models for predicting ICRF heating in future tokamak machines. One such example is the prediction that 50MW of 2.5% ^3He minority heating would give a “direct” route to ignition in ITER with more than 70% ion heating [43].

5.2 D-T Fusion Power and Q

One of the main objectives of DTE1 was the production and investigation of high fusion power plasmas under ELM-free and ELMy H-mode and optimised shear conditions. Figure 21 shows typical best pulses in these three regimes. The highest transient fusion power of 16.1MW was obtained in high current, high magnetic field ELM-free H-mode discharges, in which the current was ramped-down to delay Outer Modes (see section 3.2). The discharge reached $Q_{\text{in}}=P_{\text{fus}}/P_{\text{in}}=0.62$ and $Q_{\text{tot}}=P_{\text{fus}}/(P_{\text{loss}}-P_{\alpha})=0.95\pm 0.17$, the value Q_{in} would reach if the same plasma conditions could be achieved in steady-state (see [36]). ELMy H-mode discharges produced 4MW steady-state fusion power with $Q_{\text{in}}=0.18$ and a fusion energy of 22MJ. Finally, in the optimised shear mode of operation 8.2MW fusion power were produced in high current, high field discharges. This was somewhat below the performance extrapolated from the best discharges in D-D (projection $\approx 12\text{MW}$), due to the fact that the relatively tight neutron budget allowed only limited development of the optimised shear scenario in D-T (in particular methods to raise the core density and optimise the pressure profiles with regard to MHD stability).

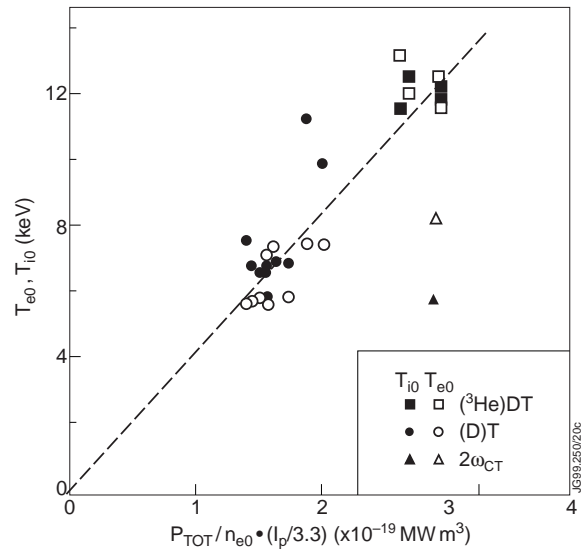


Fig. 20 Central ion and electron temperature plotted against power per particle, corrected for values of plasma current different to 3.3MA.

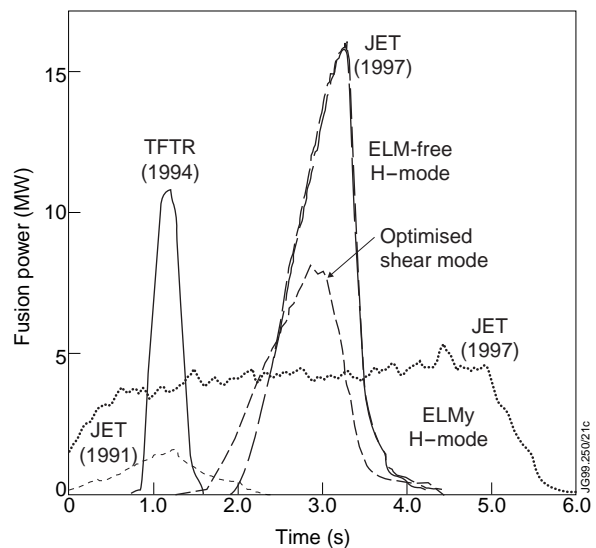


Fig. 21 Transient (16MW) and steady-state (4MW) D-T fusion power in the JET DTE1 campaign (1997) and comparison with the best TFTR result (1994) and the JET PTE (1991).

5.3 Alpha-particle Driven Alfvén Eigenmodes

The investigation of Alfvén Eigenmodes (AE) in tokamak plasmas is motivated by the potential of such waves to eject energetic α -particles from the core of a fusion reactor, leading to a reduction in the α -particle heating efficiency and a possible damage of the first wall. The study of AEs in JET during DTE1 has demonstrated that these modes can be destabilised by energetic ions produced by ICRF or NB heating [44]. On the other hand, no evidence of α -particle driven AEs has been observed in the record fusion power discharges [36]. The latter is in agreement with stability calculations (Fig. 22) which show that the normalised α -particle pressure in these discharges is a factor of two below the instability threshold for the least damped AEs ($n \approx 5$) [45].

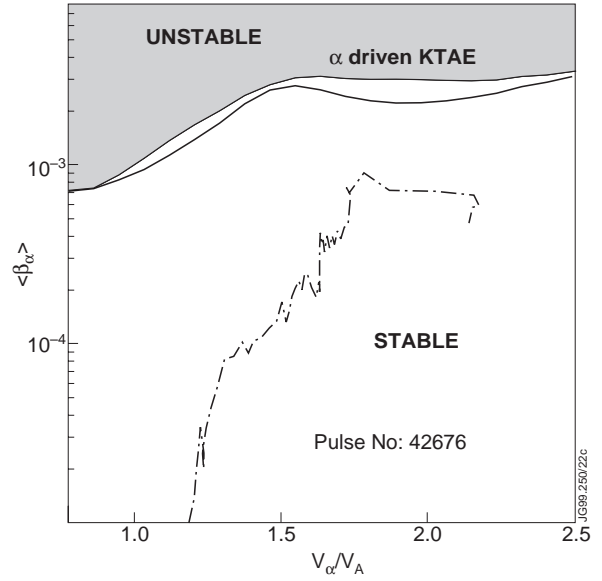


Fig. 22 Instability zone for α -particle driven non-ideal KTAEs for the conditions of the high fusion power pulse Pulse No. 42676 (the solid line shows the instability boundary without stabilising effect of the NB injection) and the actual discharge trajectory for this pulse.

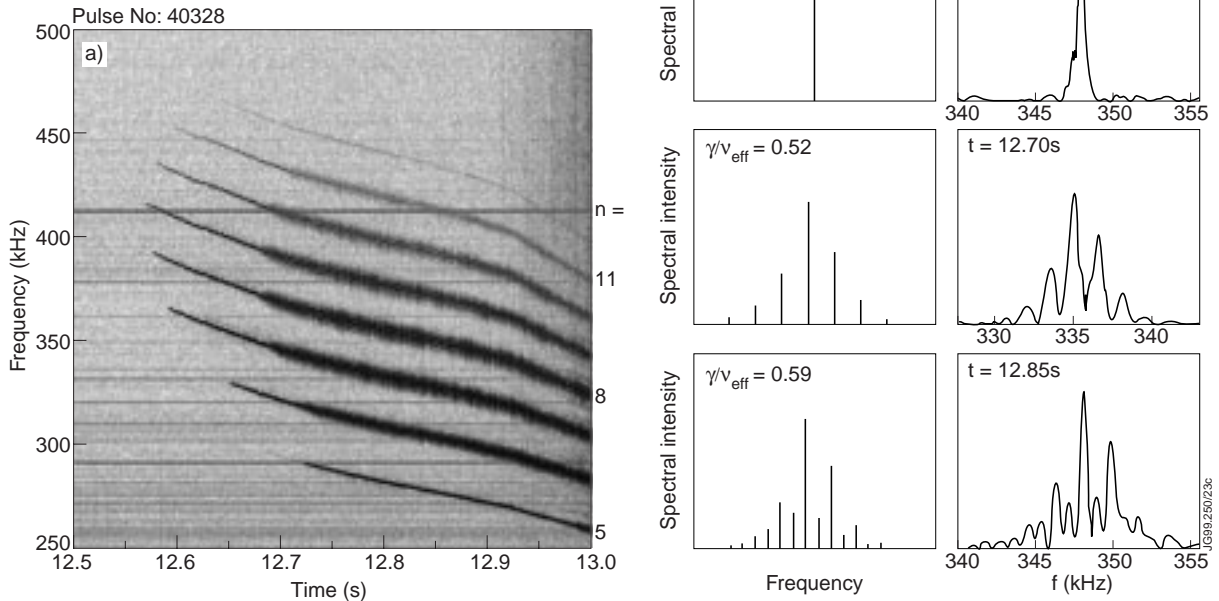


Fig. 23 Frequency splitting of fast particle (from H-minority ICRF) driven Alfvén Eigenmodes. a) Measured magnetic fluctuation spectra, and comparison of b) calculated power spectrum (left) and c) experimental spectrum of the $n=7$ mode of a).

Another interesting example of the interplay between experimental observations and theoretical interpretation is shown in Fig. 23. As mentioned above, fast particle driven AEs are observed in JET when the ICRF heating power exceeds a certain critical value (typically 4MW of H-minority ICRH, superimposed on sub-Alfvénic NB heating). The measured magnetic fluctuation spectra of these AE modes (Fig. 23a) show a splitting of the mode frequencies (corresponding to toroidal mode numbers $n=5$ to 12 shifted by the Doppler effect due to the plasma rotation) into multiple frequencies (Fig. 23c) and this has subsequently been explained theoretically [46] in terms of the non-linear evolution of these AE modes (Fig. 23b).

5.4 Demonstration of Alpha Particle Heating

One of the most important objectives of DTE1 was an unambiguous demonstration of α -particle heating. To separate the α -particle heating from possible isotope effects on energy confinement, a series of specially designed hot ion ELM-free H-mode pulses was carried out in which the D-T mixture was varied from pure deuterium to almost pure tritium while all other parameters were kept constant [47]. Comparing the pure deuterium and pure tritium ends of this scan revealed that the global energy confinement time in ELM-free H-modes has no, or only a very weak, isotope dependence; this simplifies the interpretation of the α -particle heating experiment.

One way of presenting the results of the α -particle heating experiment is depicted in Fig. 24, which is a plot of the central electron temperature versus the calculated α -particle heating power for the set of pulses in the D-T mixture scan. The highest electron temperature shows a clear

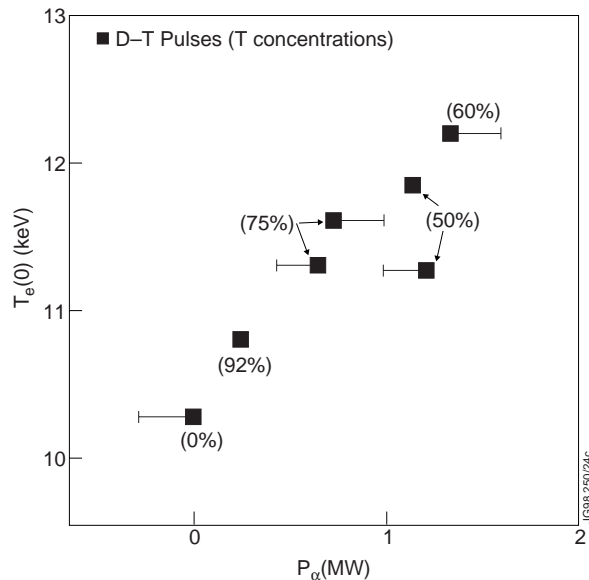


Fig. 24 Central electron temperature versus alpha particle heating power. The bars indicate the variation in NB power compared to the 92% tritium reference pulse. The figures in brackets are the tritium concentrations $n_T/(n_T+n_D)$.

correlation with the maximum α -particle heating power and with the optimum D-T plasma mixture (40:60). A regression fit to the data gives a change in central electron temperature of 1.3 ± 0.23 keV with 1.3 MW of alpha particle heating power.

These results are a clear demonstration of the self-heating of a D-T plasma by the α -particles produced by fusion reactions. A comparison with ICRF heating of a H-minority species in a plasma under similar conditions showed that the α -particle heating was as effective. This is a strong indication that, in the absence of MHD instabilities, the confinement and slowing down of α -particles and their heating effect are classical and that there are no unexpected effects which might prevent ignition in a device such as ITER.

6. CONCLUSIONS AND IMPLICATIONS

So, what has been learnt from the JET experiments of the last years, where does fusion physics understanding stand, and which important questions are still open?

With regard to confinement, the JET D-T “Wind Tunnel” experiments have shown that global confinement in ELMy H-modes is close to gyro-Bohm scaling and extrapolates to ignition in ITER. However, the question remains whether the profiles in ITER will be the same as in JET. In addition, transport barriers such as the H-mode barrier at the plasma edge and the internal transport barrier observed in optimised (reversed) shear discharges lead to better confinement locally, modifying plasma profiles and allowing MHD limits to be reached. For H-mode plasmas the JET experiments have shown that confinement can be separated into core and edge confinement and that different scaling laws, which reflect different physics, apply to the two regions (with gyro-Bohm scaling in the plasma core).

In the area of MHD stability, the nature of most of the performance limiting instabilities has been identified (neoclassical tearing modes in ELMy H-modes, external kink modes in ELM-free H-modes and ideal pressure driven kink modes and $q=2$ ‘snakes’ in optimised shear discharges) and this has in most cases led to recipes for their avoidance. However, the final proof that high β , steady-state tokamak operation, which requires a high fraction of bootstrap current, is possible, is still to come: Will it be possible to produce and maintain current and pressure profiles consistent with transport and with the requirements of stability and bootstrap current?

Also, understanding the edge and divertor physics has made big steps forward. The three stage programme of progressively more closed JET divertors (Mark I, IIA and IIGB) has demonstrated the expected beneficial effects of divertor closure, in particular higher divertor neutral pressures (easing particle removal) and a reduction in Z_{eff} in the bulk plasma. In addition it has been shown that radiation and CX neutrals (in a detached divertor plasma) can reduce the average power load on the divertor targets of a Next Step device to acceptable levels. However, two important issues remain. The problem of the extremely high transient power deposition on the divertor targets during Type I ELMs (which are a feature of the H-modes with the best confinement properties) and its scaling to larger machines, and the issue of an adequate target material for Next Step devices, with carbon seeming unacceptable because of its high tritium retention and large erosion rate.

The JET D-T experiments during 1997 (DTE1) have been extremely successful and broken all records in fusion performance (16MW transient fusion power and $Q=Q_{\text{fus}}/Q_{\text{in}}=0.62$). More importantly they have allowed a clear demonstration of α -particle heating consistent with classical expectations (heating efficiency similar to H-minority ICRF heating) and have shown that, in agreement with stability calculations, no α -particle driven TAE modes were excited in these high performance discharges. However, a full assessment of α -particle effects will require plasmas with $Q>1$ sustained for a few seconds, which is the goal for DTE2 experiments at the end of JET operation.

In summary, substantial progress in physics understanding has been made on JET and other tokamak experiments and this should be sufficient for extrapolation to a Next Step machine based on ELMy H-mode operation, provided the machine has sufficient margins. However, more detailed information is required to build a Next Step device closer to operational limits and to base its design on advanced tokamak scenarios leading to a cheaper device. In this quest JET has still a lot to offer and its continued use will be vital for defining the operating conditions of a Next Step tokamak.

ACKNOWLEDGEMENTS

The author gratefully acknowledges clarifying discussions with G. Conway, J.G. Cordey, G. Huysmans, J. Lingertat, G.F. Matthews and in particular M.L. Watkins.

REFERENCES

- [1] JET TEAM (presented by P. J. LOMAS), in Fusion Energy 1996 (Proc. 16th Int. Conf. Montreal, Canada, 1996) Vol. 1, IAEA, Vienna (1997) 239.
- [2] BHATNAGAR, V.P. et al., Nucl. Fus. **39** (1999) 353.
- [3] JET TEAM (presented by C. GORMEZANO), in Fusion Energy 1996 (Proc. 16th Int. Conf. Montreal, Canada, 1996) Vol. 1, IAEA, Vienna (1997) 487.
- [4] AYMAR, R., et al., in Fusion Energy 1996 (Proc. 16th Int. Conf. Montreal, 1996), Vol. 1, IAEA, Vienna (1997) 3.
- [5] KEILHACKER, M. and the JET Team, Fusion Engineering and Design (1999), accepted for publication (Invited paper SOFE Conf., Marseille, September 1998).
- [6] JET TEAM (presented by J.G. Cordey), 17th IAEA Conference 1998, Yokohama, Paper CN-69/EX7/1.
- [7] ITER Confinement Data Base and Modelling Working Group (presented by J.G. Cordey), Plasma Phys. Control. Fusion **39** (1997) B115.
- [8] ITER Confinement Database and Modelling Expert Group (presented by T. Takizuka), in Fusion Energy 1996 (Proc. 16th Int. Conf. Montreal, Canada, 1996) Vol. 2, IAEA, Vienna (1997) 795.
- [9] HORTON, L. et al., this Conference TL14.
- [10] JACQUINOT, J. et al., Plasma Phys. Control. Fusion **30** (1988) 1467.
- [11] HUGON, M. et al., Nucl. Fusion **32** (1992) 33.
- [12] GORMEZANO, C. et al., this Conference TL25.
- [13] CHALLIS, C. et al., this Conference Or18.
- [14] SIPS, A.C.C. et al., this Conference P1.027.
- [15] BURRELL, K.H., Phys. Plasmas **4** (1997) 1499.
- [16] CONWAY, G.D. et al., this Conference P1.017.
- [17] JET TEAM (presented by G. Huysmans), 17th IAEA Conf. 1998, Yokohama, Paper CN-69/EXP3/03 (an extended version of this paper has been accepted for publication in Nucl. Fus.).

- [18] BUTTERY, R.J. et al., this Conference P1.003.
- [19] LA HAYE, R.J. et al., in Fusion Energy 1996 (Proc. 16th Int. Conf. Montreal, Canada, 1996) Vol. 1, IAEA, Vienna (1997) 747.
- [20] GUENTER, S. et al., this Conference TL15.
- [21] HUYSMANS, G.T.A. et al., Nucl. Fus. **38** (1998) 179.
- [22] NAVE, M.F.F. et al., accepted for publication in Nucl. Fus. (1999)
- [23] HUYSMANS, G.T.A. et al., accepted for publication in Nucl. Fus. (1999)
- [24] HENDER, T.C. et al., this Conference Or25.
- [25] JET TEAM (presented by G.C. Vlases), in Fusion Energy 1996 (Proc. 16th Conf. Montreal, Canada, 1996) Vol. 2, IAEA, Vienna (1997) 371.
- [26] STORK, D. et al., this Conference P1.024.
- [27] REITER, D. and G. WOLF, Nucl. Fus. **30** (1990) 1241.
- [28] BOSCH, H.S. et al., Plasma Physics and Controlled Nuclear Fusion Research 1996, IAEA, Vienna 1997, Vol. 1, 809.
- [29] WADE, M.W. et al., Phys. Rev. Lett. **74** (1995) 2702.
- [30] LINGERTAT, J., 4th European Fusion Physics Workshop, Stockholm, 11-13 December 1996.
- [31] GUO, H.Y. et al., this Conference P1.037.
- [32] KEILHACKER, M. et al., Plasma Physics and Controlled Nuclear Fusion Research 1990, IAEA, Vienna 1991, Vol. 1, 345.
- [33] WADE, M.W. et al., Nucl. Fus. **38** (1998) 1839.
- [34] BOSCH, H.S. et al., Phys. Rev. Lett. **76** (1996), 2499.
- [35] CHANKIN, A.V. et al, this Conference P1.040.
- [36] KEILHACKER, M. et al., and the JET TEAM, Nucl. Fusion **39** (1999) 209.
- [37] COAD, J.P. et al., this Conference Or14.
- [38] VON KEUDEL, A., submitted to Nucl. Fus.
- [39] JET TEAM, Nucl. Fus. **32** (1992) 187.
- [40] JACQUINOT, J. et al., and the JET TEAM, Nucl. Fusion **39** (1999) 235.
- [41] GIBSON, A. and the JET TEAM, Physics of Plasmas **5** (1998) 1839.
- [42] START, D.F.H. et al., Phys. Rev. Lett. **80** (1998) 4681.
- [43] START, D.F.H. et al., in Europhysics Conference Abstracts (Proc. of the 24th EPS Conference on Controlled Fusion and Plasma Physics, Berchtesgaden, Germany, 1997), Vol. 21A, Part 1, 141.
- [44] FASOLI, A. et al., Plasma Phys. Control. Fusion **39** (1997) B287.
- [45] SHARAPOV, S.E. et al., Nucl. Fusion **39** (1999) 373.
- [46] FASOLI, A. et al., Phys. Rev. Lett. **81** (1998) 5564.
- [47] THOMAS, P.R. et al., Phys. Rev. Lett. **80** (1998) 5548.